Structural Evolution, Sequential Oxidation, and Chemical Bonding in Tritantalum Oxide Clusters: $Ta_3O_n^-$ and Ta_3O_n ($n = 1-8$)

Hua-Jin Zhai,[†] Bin Wang,[‡] Xin Huang,*[,‡] and Lai-Sheng Wang*[,†]

Department of Physics, Washington State University, 2710 University Drive, Richland, Washington 99354, Chemical & Materials Sciences Division, Pacific Northwest National Laboratory, MS K8-88, P.O. Box 999, Richland, Washington 99352, Department of Chemistry, Fuzhou University, Fuzhou, Fujian 350108, P. R. China, and State Key Laboratory of Structural Chemistry, Fuzhou, Fujian 350002, P. R. China

Received: June 11, 2009; Revised Manuscript Received: July 28, 2009

We report a combined photoelectron spectroscopy (PES) and density functional theory (DFT) study on a series of tritantalum oxide clusters, $Ta_3O_n^-$. Well-resolved PES spectra are obtained for $Ta_3O_n^-$ ($n = 1-8$) at several detachment photon energies, yielding electronic structure information which is used for comparison with the DFT calculations. A trend of sequential oxidation is observed as a function of O content until $Ta_3O_8^-$, which is a stoichiometric cluster. Extensive DFT calculations are performed in search of the lowest energy structures for both the anions and neutrals. The first three O atoms are shown to successively occupy the bridging sites in the Ta_3 triangle. The next three O atoms each occupy a terminal site, with the seventh and eighth O atoms forming a double-bridge and a double-terminal, respectively. The $Ta_3O_7^-$ anion is found to possess a localized electron pair on a single Ta center, making it an interesting molecular model for Ta^{3+} surface sites. Molecular orbital analyses are performed to elucidate the chemical bonding in the $Ta_3O_n^-$ clusters.

1. Introduction

Group VB metal oxides are used as catalysts in numerous industrial processes.[1,2] In contrast to vanadium and niobium oxides, current understanding of the catalytic properties of tantalum oxides is rather limited.[2,3] Evidence has been shown that tantalum oxides are strong catalytic promoters, i.e., enhancing the activity and selectivity and prolonging the catalyst life when a small amount of tantalum oxides is added to known catalysts.[2] An understanding at the molecular level of the roles that tantalum oxides can play in catalysis and comparative studies of tantalum oxides versus vanadium and niobium oxides can help the design of better catalysts. Gas-phase clusters, which possess controlled and well-defined structures and atomic connectivity, have been used as molecular models to mimic the surface catalytic sites and provide fundamental mechanistic insights for catalysts.[4]

Gas-phase studies on tantalum oxide clusters have been relatively scarce,[5−11] although the TaO diatomic species has been extensive studied both experimentally[12] and theoretically.[13] Reactions of $Ta_mO_n^{\pm}$ clusters with hydrocarbon molecules have been conducted.[5] Photodissociation studies on $M_mO_n^+$ (M = V, Nb, Ta) showed enhanced stability for certain cluster sizes such as $M_2O_4^+$, $M_3O_7^+$, and $M_4O_9^+$.[8] Single photon ionization experiments at 26.5 eV were performed on neutral M_mO_n (M = V, Nb, Ta) clusters, and the Ta_2O_5, Ta_3O_7, and Ta_4O_{10} clusters were shown to be most abundant.[9] Infrared multiphoton dissociation spectroscopy showed a fragmentation channel of atomic oxygen loss for $Ta_3O_8^+$ and suggested the involvement of a peroxo unit in the cation.[7] However, the electronic and structural properties of tantalum oxide clusters remain poorly understood. To our knowledge, the only photoelectron spectroscopy (PES) studies available are those of Bowen and co-workers[11] on TaO_n^- ($n = 1-3$) at 355 nm and Leopold and co-workers[6] on Ta_3O^- at 488 nm, in addition to our prior PES studies on $Ta_3O_3^-$ and $Ta_4O_{10}^-$.[14,15]

We have been interested in developing cluster models[15−17] for early transition metal oxide catalysts and in elucidating the chemical bonding in novel oxide clusters.[14,18,19] The discovery of the δ bond by Cotton and co-workers[20] led to the development of a new branch of inorganic chemistry on metal−metal multiple bonds over the past 40 years.[21−25] The recent synthesis of a Cr_2 compound[22] with a quintuple bond ($\sigma^2\pi^4\delta^4$) generated renewed interest in the field.[24−26] Delocalized multicenter bonding in transition metal systems also raises the possibility for d-orbital aromaticity[18,27] and in particular δ-aromaticity.[14,19,28,29] In a recent study we found a δ-aromatic $Ta_3O_3^-$ (D_{3h}, $^1A_1'$) cluster, which represents a new mode of chemical bonding.[14] In the current contribution, we report a combined PES and density functional theory (DFT) study on the electronic and structural properties and chemical bonding of a series of trinuclear tantalum oxide clusters, $Ta_3O_n^-$ ($n = 1-8$). We are interested in examining how the O ligands are successively bonded to the Ta_3 core and the competition between bridging, terminal, and capping O ligands. These clusters with tunable oxidation states may also provide insight into the structure and bonding in synthetic trinuclear Ta_3 compounds.[30]

2. Experimental and Computational Methods

2.1. Photoelectron Spectroscopy. The experiment was carried out using a magnetic-bottle PES apparatus equipped with a laser vaporization cluster source, details of which have been described elsewhere.[31] Briefly, the $Ta_mO_n^-$ clusters were produced by laser vaporization of a tantalum disk target in the presence of a He carrier gas seeded with 0.01% O_2 for $Ta_3O_n^-$ ($n = 1-6$) or 0.5% O_2 for $Ta_3O_n^-$ ($n = 7, 8$). The cluster anions were analyzed using a time-of-flight mass spectrometer, and the $Ta_3O_n^-$ ($n = 1-8$) clusters were each mass-selected and

* To whom correspondence should be addressed. E-mail: xhuang@fzu.edu.cn (X.H.); ls.wang@pnl.gov (L.-S.W.).
[†] Washington State University and Pacific Northwest National Laboratory.
[‡] Fuzhou University and State Key Laboratory of Structural Chemistry.

10.1021/jp905478w CCC: $40.75
Published on Web 08/14/2009

decelerated before being photodetached. Four detachment photon energies were used in the present work: 532 nm (2.331 eV), 355 nm (3.496 eV), 266 nm (4.661 eV), and 193 nm (6.424 eV). Effort was made to choose colder clusters (i.e., those with long resident times in the nozzle) for photodetachment, which was shown previously to be important for obtaining high quality PES data.[32] Photoelectrons were collected at nearly 100% efficiency by the magnetic bottle and analyzed in a 3.5 m long electron flight tube. PES spectra were calibrated using the known spectra of Au^- and Rh^-, and the energy resolution of the apparatus was $\Delta E/E \sim 2.5\%$, that is, ~25 meV for 1 eV electrons.

2.2. Density Functional Calculations. The theoretical calculations were performed at the DFT level using the B3LYP hybrid functional.[33−35] A number of structural candidates including different spin states and initial structures were evaluated, and the search for the global minima was performed using analytical gradients with the Stuttgart relativistic small core basis set and efficient core potential[36,37] augmented with two f-type and one g-type polarization functions [$\zeta(f) = 0.210$, 0.697; $\zeta(g) = 0.472$] for Ta as recommended by Martin and Sundermann[38] and the aug-cc-pVTZ basis set for oxygen.[39,40] Scalar relativistic effects, that is, the mass velocity and Darwin effects, were taken into account via the quasirelativistic pseudopotentials. Vibrational frequency calculations were performed at the same level of theory to verify the nature of the stationary points. Vertical electron detachment energies (VDEs) were calculated using the generalized Koopmans' theorem by adding a correction term to the eigenvalues of the anion.[41] The correction term was calculated as $\delta E = E_1 - E_2 - \varepsilon_{HOMO}$, where E_1 and E_2 are the total energies of the anion and neutral, respectively, in their ground states at the anion equilibrium geometry and ε_{HOMO} corresponds to the eigenvalue of the highest occupied molecular orbital (HOMO) of the anion. All calculations were performed with the Gaussian 03 software package.[42] Three-dimensional contours of the molecular orbitals (MOs) were visualized using the VMD software.[43]

3. Experimental Results

The photoelectron spectra of $Ta_3O_n^-$ ($n = 1-8$) at different photon energies are presented in Figures 1−7. The 193 nm PES data of the series are compared in Figure S1 in the Supporting Information. The observed transitions are labeled with letters and the measured ground-state adiabatic detachment energies (ADEs) and VDEs are given in Table 1. All observed VDEs for the excited states are tabulated in the Supporting Information (Tables S1−S3).

3.1. Ta_3O^- and $Ta_3O_2^-$. The 532 nm spectrum of Ta_3O^- (Figure 1a) reveals the ground-state band X, which exhibits a short vibrational progression with a spacing of 710 ± 30 cm^{-1}. The 0−0 transition at 1.583 ± 0.015 eV defines the ground-state VDE and ADE, which is also the electron affinity of Ta_3O neutral. At 355 nm (Figure 1b), three more electronic states (A, B, and C) are resolved at 1.99, 2.06, and 2.63 eV, respectively. A partial D band is also observed at 355 nm. Bands A and B are closely spaced within 0.1 eV, whereas band C is relatively sharp and intense. A prior PES study at 488 nm by Leopold and co-workers[6] has characterized bands X, A, and B at a higher resolution, yielding a more accurate electron affinity (1.583 ± 0.010 eV) and ground-state vibrational frequency (710 ± 15 cm^{-1}). The 266 and 193 nm spectra (Figure 1c,d) further reveal bands D (3.10 eV) and E (4.40 eV). Band D appears broad and asymmetric, probably containing unresolved multiple transitions. In addition, continuous electron signals are observed at the high binding energy side at both 266 and 193 nm.

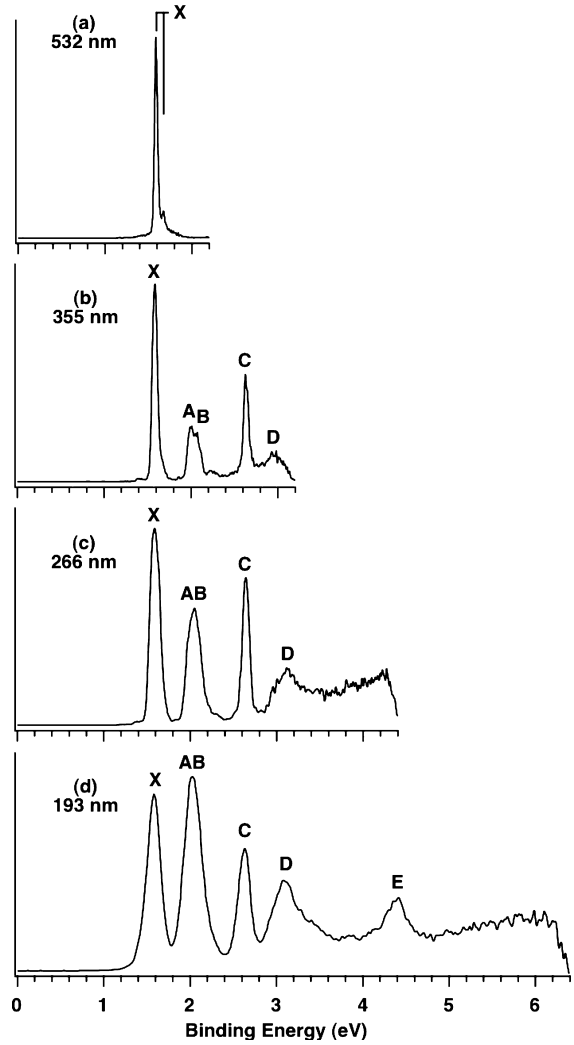

Figure 1. Photoelectron spectra of Ta_3O^- at (a) 532 nm (2.331 eV), (b) 355 nm (3.496 eV), (c) 266 nm (4.661 eV), and (d) 193 nm (6.424 eV). The vertical lines in part a represent vibrational structures.

The 532 nm spectrum of $Ta_3O_2^-$ (Figure 2a) reveals the ground state X, which is substantially broader than that of Ta_3O^- (Figure 1a). The ground-state VDE is measured to be 1.675 eV from the band maximum. Since no vibrational structures are resolved for band X, the ground-state ADE is evaluated by drawing a straight line along the leading edge of band X and then adding the instrumental resolution to the intersection with the binding energy axis. Although this is an approximate procedure, we are able to obtain a consistent ADE from the well-defined spectral onsets of band X at different photon energies. The ADE thus evaluated for $Ta_3O_2^-$ is 1.62 eV. The 355 and 266 nm spectra (Figure 2b,c) reveal three additional bands A, B, and C at 2.18, 2.57, and 3.20 eV, respectively. Band C is broad and asymmetric, similar to band D for Ta_3O^- (Figure 1c). Continuous electron signals are observed beyond band C at 193 nm (Figure 2d), where a broad band D (~4.9 eV) is tentatively labeled.

3.2. $Ta_3O_3^-$ and $Ta_3O_4^-$. We recently reported the 193 nm spectrum of $Ta_3O_3^-$ in a brief communication,[14] which exhibits three prominent bands X, A, and B followed by an extended continuous tail beyond ~3.7 eV (Figure 3c). Relative to bands A and B, band X is much more intense and shows a discernible splitting. In the current study, we have obtained higher resolution spectra at 355 and 266 nm (Figure 3a,b). The splitting in band X is well-resolved into two components (2.253 and 2.376 eV),

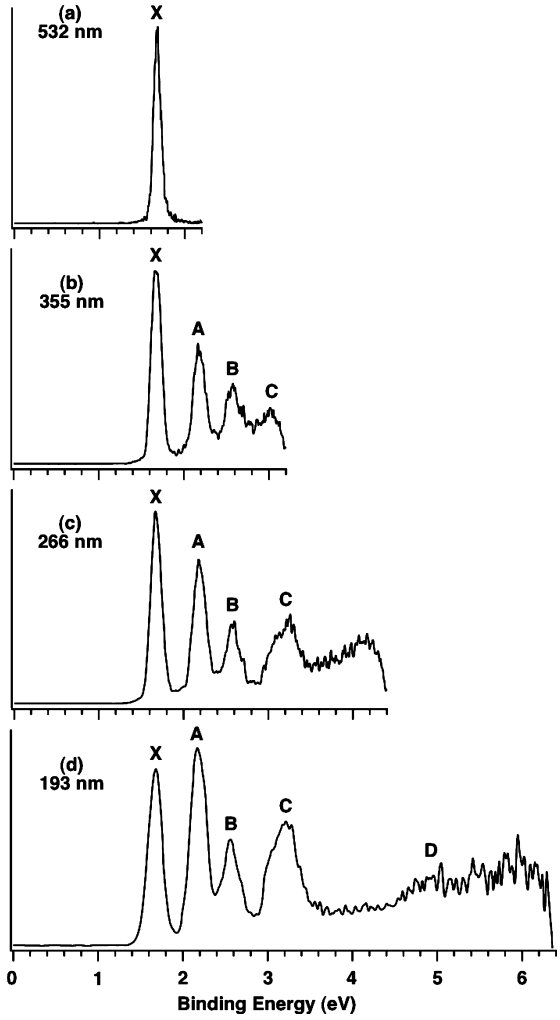

Figure 2. Photoelectron spectra of $Ta_3O_2^-$ at (a) 532 nm, (b) 355 nm, (c) 266 nm, and (d) 193 nm.

defining a splitting of 0.123 eV. Two additional weak bands a (2.70 eV) and b (3.10 eV) are also revealed, probably due to multielectron (shakeup) transitions, which have been observed quite definitively in a number of cluster systems previously.[44] We note that the PES bands for $Ta_3O_3^-$ are relatively sharp (Figure 3), similar to those for Ta_3O^- (Figure 1), whereas those for the rest of the $Ta_3O_n^-$ species are more diffused.

The 355 nm spectrum of $Ta_3O_4^-$ (Figure 4a) shows two electronic states: X (2.40 eV) and A (2.70 eV). An electron affinity of 2.29 eV is evaluated for Ta_3O_4 from the sharp onset of band X. At 266 nm (Figure 4b) a broad band B (3.31 eV) is revealed. No prominent transitions exist in the 3.6−4.6 eV region as shown in the 193 nm spectrum (Figure 4c). A broad band C clearly appears at 5.04 eV, followed by congested and intense signals beyond 5.2 eV.

3.3. $Ta_3O_5^-$ and $Ta_3O_6^-$. The 355 nm spectrum of $Ta_3O_5^-$ (Figure 5a) reveals an intense ground-state transition X with an ADE (2.25 eV) and VDE (2.33 eV) similar to that of $Ta_3O_4^-$ (Table 1). The 266 nm spectrum (Figure 5b) further shows two very broad bands A and B, which become better defined at 193 nm (Figure 5c). Band A at 3.14 eV (Table S2) is very broad, which likely contains unresolved multiple transitions. Band C (4.86 eV) is similar to that in $Ta_3O_4^-$, whereas band B (3.91 eV) is weaker and may originate from an isomer.

The PES spectra of $Ta_3O_6^-$ (Figure 6) appear congested and broad. Four broad bands (X, A, X′, and A′) are labeled and tentatively assigned to two isomers (below). Bands X (3.44 eV)

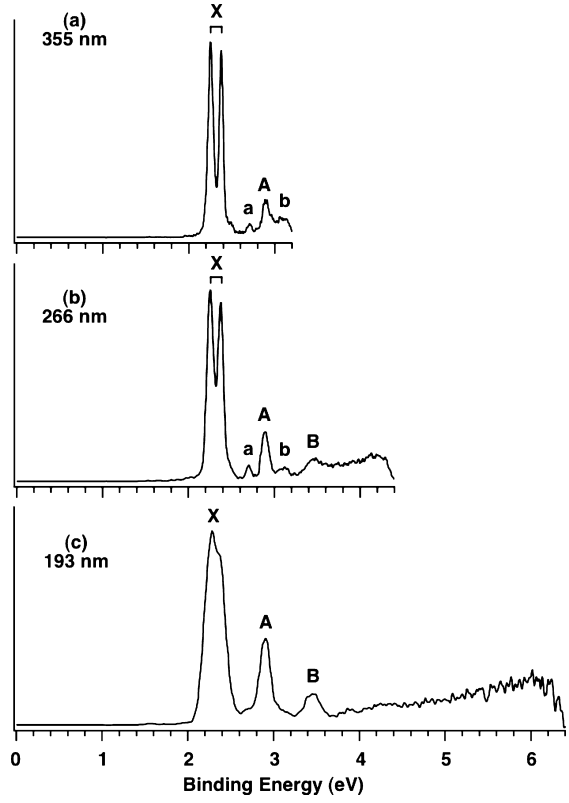

Figure 3. Photoelectron spectra of $Ta_3O_3^-$ at (a) 355 nm, (b) 266 nm, and (c) 193 nm.

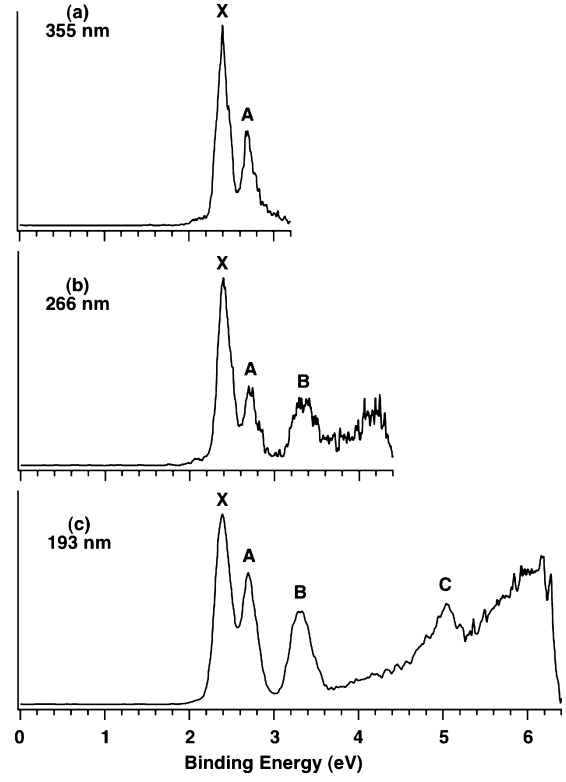

Figure 4. Photoelectron spectra of $Ta_3O_4^-$ at (a) 355 nm, (b) 266 nm, and (c) 193 nm.

and X′ (3.12 eV) represent the ground states for the isomers. The electron affinities for the neutrals are estimated to be ∼3.2 and ∼2.9 eV, respectively.

3.4. $Ta_3O_7^-$ and $Ta_3O_8^-$. Due to their high electron binding energies, the spectra of $Ta_3O_7^-$ and $Ta_3O_8^-$ are only measured

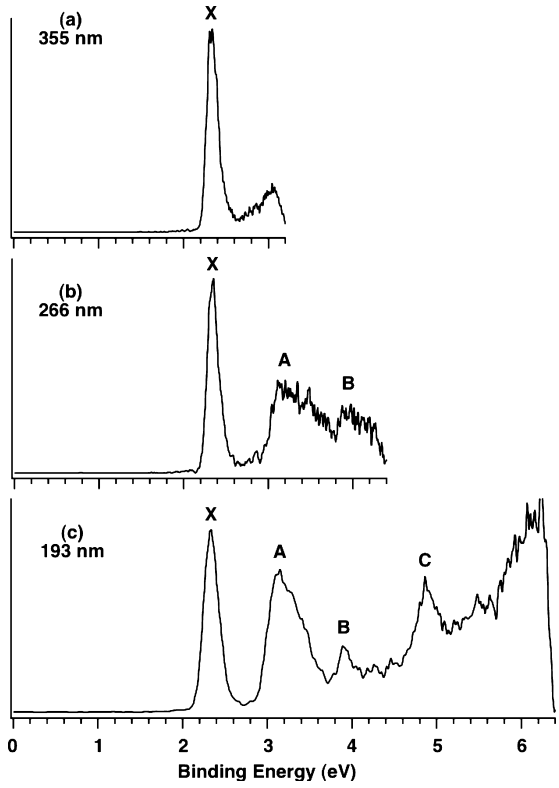

Figure 5. Photoelectron spectra of $Ta_3O_5^-$ at (a) 355 nm, (b) 266 nm, and (c) 193 nm.

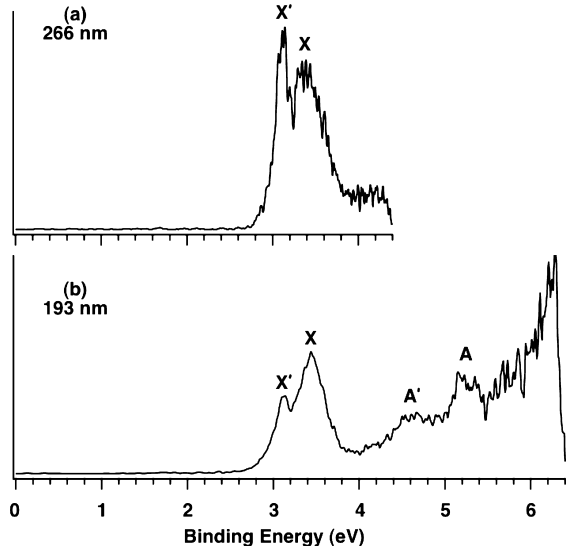

Figure 6. Photoelectron spectra of $Ta_3O_6^-$ at (a) 266 nm and (b) 193 nm.

at 193 nm, as shown in Figure 7. The ground state X of $Ta_3O_7^-$ (ADE, 3.62 eV; VDE, 3.92 eV) is broad, followed by a large energy gap and an intense band A (Figure 7a). Band A is located at such a high binding energy that the full bandwidth may not be accessed at 193 nm. The estimated ADE for band A is ~6.0 eV, defining an X−A energy gap of ~2.4 eV. The electron binding energy for $Ta_3O_8^-$ is very high (Figure 7b). The ground state X exhibits a partially resolved vibrational progression (~810 cm^{-1}). The VDE is measured as 5.81 eV from the band maximum, whereas the ADE is defined by the 0−0 transition at 5.51 eV.

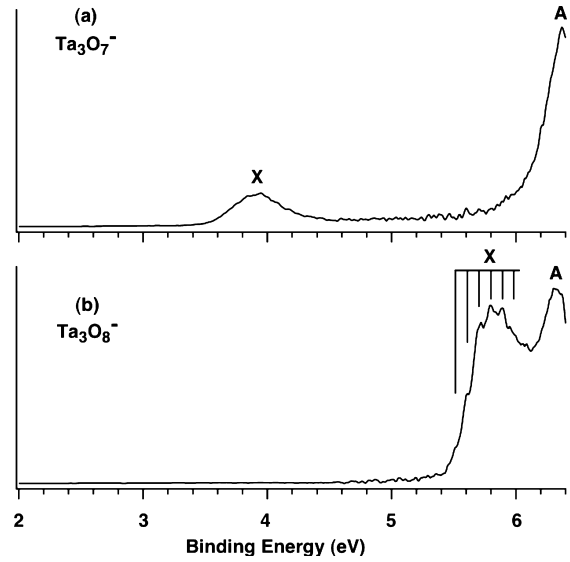

Figure 7. Photoelectron spectra of (a) $Ta_3O_7^-$ and (b) $Ta_3O_8^-$ at 193 nm. The vertical lines in part b represent vibrational structures.

TABLE 1: Experimental Adiabatic (ADE) and Vertical (VDE) Detachment Energies of $Ta_3O_n^-$ ($n = 1-8$) and Comparison with the Calculated VDEs from the Lowest-Energy Anion Structures at the B3LYP Level of Theory

	ADE (exptl)[a−c]	VDE[a,b] (exptl)	anion state	VDE[a] (theor)
Ta_3O^-	1.583 (15)[d,e]	1.583 (15)	C_{2v} ($^1A_1$)	1.36
$Ta_3O_2^-$	1.62 (3)	1.675 (15)	C_2 (^1A)	1.44
$Ta_3O_3^-$	2.22 (3)	2.253 (15)	D_{3h} ($^1A_1'$)	2.24
$Ta_3O_4^-$	2.29 (3)	2.40 (3)	C_s ($^1A'$)	2.23
$Ta_3O_5^-$	2.25 (3)	2.33 (3)	C_2 (^1A)	2.02[f]
$Ta_3O_6^-$	~3.2[g]	3.44 (5)	C_s ($^1A'$)	3.32[f]
	~2.9[g]	3.12 (5)	C_{3v} ($^3A_1$)	3.25
$Ta_3O_7^-$	3.62 (5)	3.92 (5)	C_1 (^1A)	3.60
$Ta_3O_8^-$	5.51 (3)[d]	5.81 (3)	C_{2v} ($^1A_1$)	5.69

[a] All energies are in eV. [b] Numbers in the parentheses represent experimental uncertainties in the last digits. [c] Electron affinity of the neutral species. [d] Ground-state vibrational frequency: 710 ± 30 cm^{-1} for Ta_3O and ~810 cm^{-1} for Ta_3O_8. [e] More accurate electron affinity and vibrational frequency were reported previously: 1.583 ± 0.010 eV and 710 ± 15 cm^{-1} (ref 6). [f] Lowest energy closed-shell structure; second lowest among all calculated structures at the B3LYP level. [g] Two isomers.

4. Theoretical Results

The optimized ground-state structures and selected low-lying isomers of $Ta_3O_n^-$ and Ta_3O_n ($n = 1-8$) are presented in Figures 8 and 9, respectively. Their calculated first VDEs are compared with the experimental values in Table 1. The complete sets of experimental and computational VDEs are compared in the Supporting Information (Tables S1−S3). The simulated PES spectra from the lowest-energy anion structures are compared with experiment in Figure 10. Alternative optimized structures are shown in the Supporting Information (Figures S2−S17). The calculated first VDEs from the low-lying anion structures are compared with experiment in the Supporting Information (Table S4), and their simulated PES spectra are also compared with experiment in the Supporting Information (Figures S18−S25).

4.1. $Ta_3O_n^-$ and Ta_3O_n ($n = 1-3$). Candidate structures optimized in our search of the Ta_3O^- and Ta_3O ground states include planar and nonplanar structures with a bridging or terminal oxygen and three-dimensional ones with an oxygen

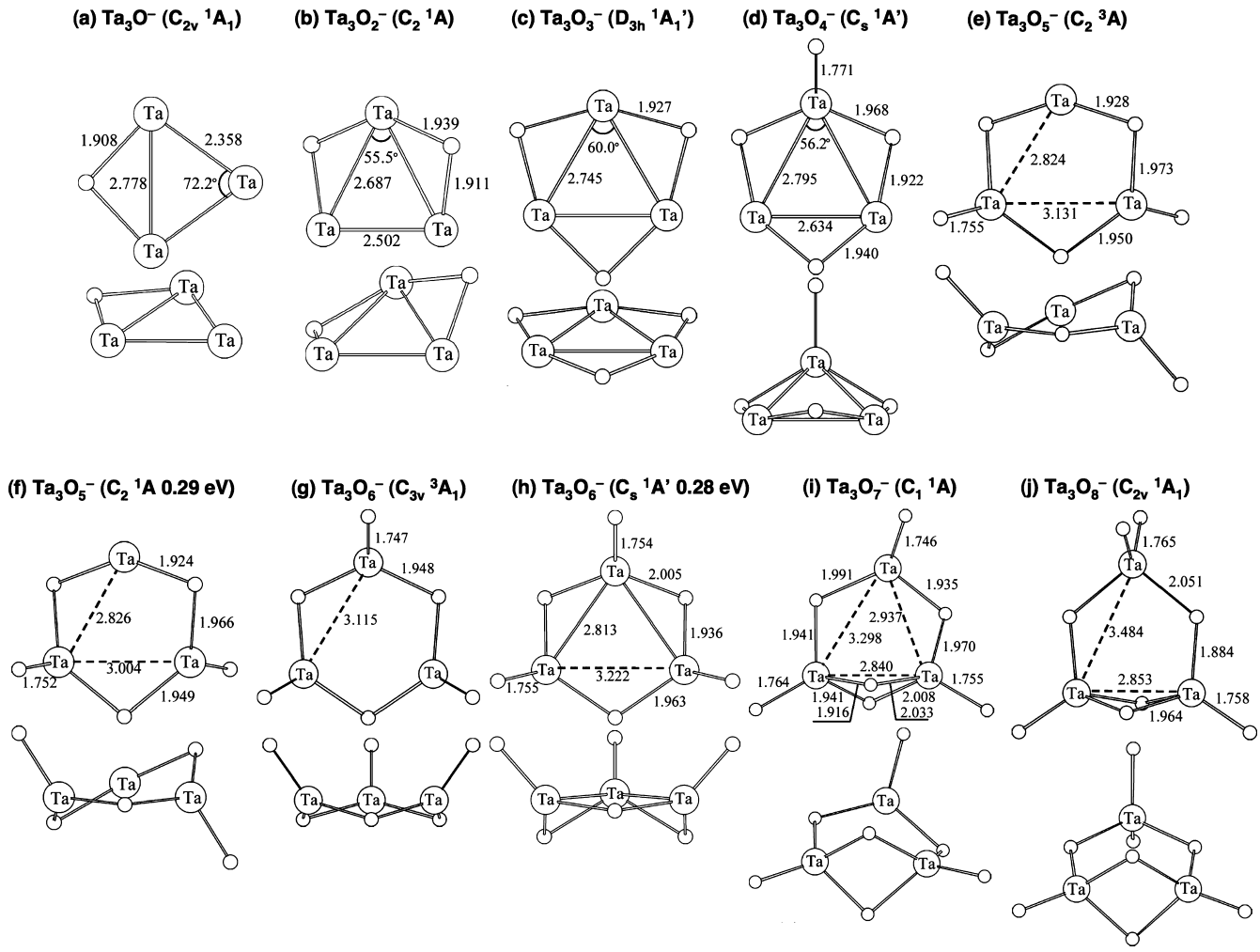

Figure 8. Optimized lowest-energy structures for the $Ta_3O_n^-$ ($n = 1-8$) clusters at the B3LYP level of theory. Low-lying singlet structures are also presented for structures (f) $Ta_3O_5^-$ and (h) $Ta_3O_6^-$. Both top and side views are shown.

atom capped on the top of the Ta_3 triangle (Figures S2 and S3, Supporting Information). Different spin states are calculated in each case. The planar Ta_3O^- (C_{2v}, $^1A_1$) and Ta_3O (C_{2v}, $^2B_2$) structures with a bridging oxygen atom are found to be the ground states as shown in Figures 8a and 9a, in agreement with those previously found by Wu et al.[10] The second lowest isomers, Ta_3O^- (C_{2v}, $^3B_2$) and Ta_3O (C_{2v}, $^4B_2$), are also planar with a bridging O atom, being 0.27 and 0.45 eV above the ground states, respectively.

A variety of structures with different symmetries and spin multiplicities are calculated for $Ta_3O_2^-$ and Ta_3O_2 (Figures S4 and S5). The $Ta_3O_2^-$ anion ground state is found to be closed-shell with C_2 (^1A) symmetry and two bridging oxygen atoms (Figure 8b). The triplet dibridged structure C_2 (^3B) is only 0.10 eV higher in energy. Among other higher energy structures, the C_1 (^3A) and C_1 (^1A) structures with one bridging and one terminal oxygen are 0.31 and 0.56 eV above the ground state, respectively. The Ta_3O_2 ground state is found as C_2 (^2A) (Figure 9b), very similar to the anion. Structures with one bridging and one terminal oxygen atom are found to be at least 0.53 eV above the neutral ground state.

Extensive search of the potential energy surfaces of $Ta_3O_3^-$ and Ta_3O_3 (Figures S6 and S7) reveals a highly symmetric planar D_{3h} ($^1A_1'$) ground state for $Ta_3O_3^-$ (Figure 8c), consistent with that reported in the recent communication.[14] A triplet C_s ($^3A''$) structure is 0.30 eV higher in energy. The ground state of Ta_3O_3 neutral is found to be C_s ($^2A'$) (Figure 9c), in which the three O atoms are slightly out of the Ta_3 plane. Two similar doublet C_s ($^2A''$) and quartet C_s ($^4A''$) states are 0.11 and 0.30 eV above the ground state, respectively.

4.2. $Ta_3O_n^-$ and Ta_3O_n ($n = 4-6$). Starting from the tribridged conformation of $Ta_3O_3^-$ and Ta_3O_3, we have considered different sites (terminal, bridging, and capping) to add the extra O atoms in search of the ground states for $Ta_3O_n^-$ and Ta_3O_n ($n = 4-6$) (Figures S8−S13). The additional oxygen atoms ($n = 4-6$) are shown to successively occupy the terminal sites (Figures 8 and 9). The $Ta_3O_4^-$ and Ta_3O_4 ground states are found to be C_s ($^1A'$) (Figure 8d) and C_s ($^2A''$) (Figure 9d), respectively, with the fourth O atom occupying a terminal site. An anion isomer C_s ($^3A''$) is only 0.14 eV above the ground state (Figure S8), whereas the lowest neutral quartet state C_s ($^4A''$) is 0.20 eV above the ground state (Figure S9).

The potential energy surfaces for $Ta_3O_5^-$ and Ta_3O_5 are rather flat with closely lying isomers near the global minimum (Figures S10 and S11). The $Ta_3O_5^-$ anion ground state is found to be triplet C_2 (^3A) (Figure 8e), with the nearest C_s ($^3A''$) and C_s ($^5A''$) states both being about 0.18 eV higher in energy. The singlet C_2 (^1A) state (Figure 8f) is 0.29 eV above the ground state. Another C_2 (^5A) isomer is also close to the ground state (by 0.30 eV). The ground state of Ta_3O_5 is C_2 (^2A) (Figure 9e), with other structures being at least 0.40 eV higher in energy.

The $Ta_3O_6^-$ ground state is found to be a crown-shaped C_{3v} ($^3A_1$) (Figure 8g). The corresponding singlet $^1A'$ state is 0.28 eV higher in energy with C_s symmetry (Figure 8h). The neutral

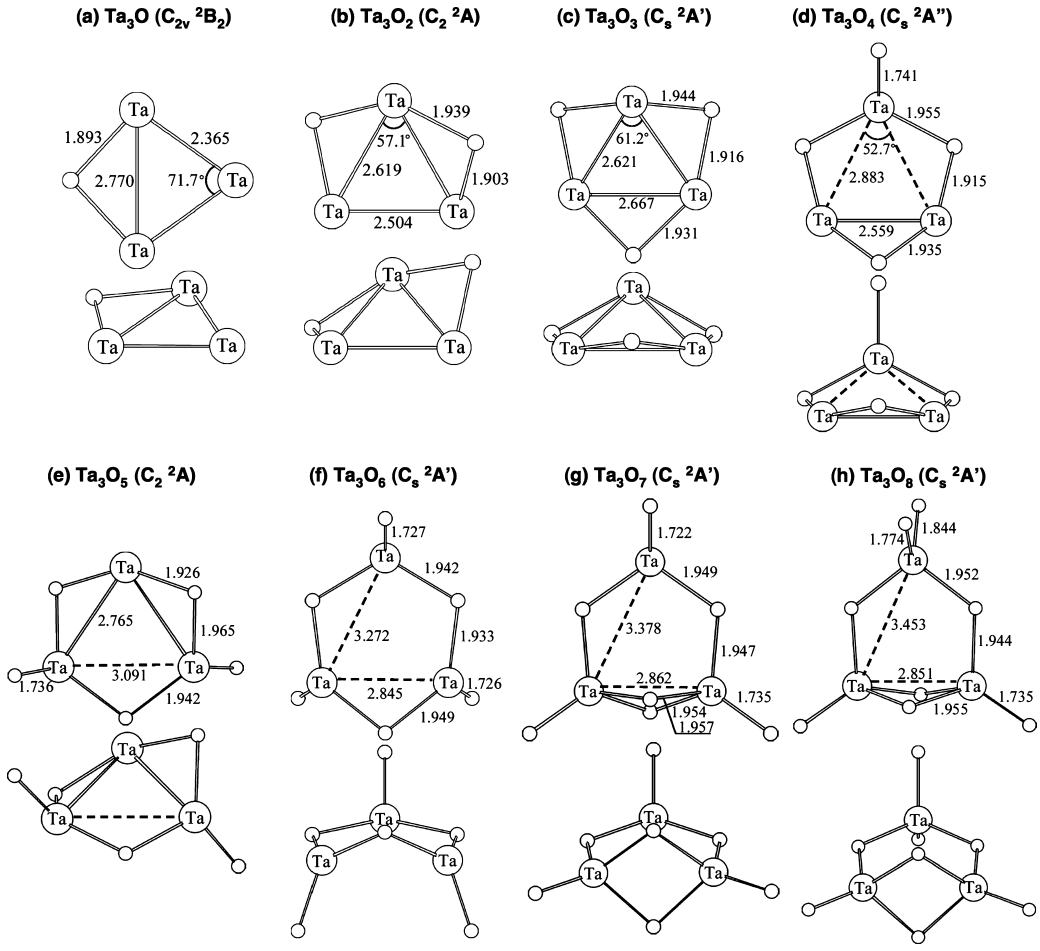

Figure 9. Optimized lowest-energy structures for Ta_3O_n ($n = 1-8$) neutral clusters at the B3LYP level of theory. Both top and side views are shown.

Ta_3O_6 ground state is found to be C_s ($^2A'$) (Figure 9f), which differs from the anion mainly in the terminal oxygen directions with two terminal oxygen atoms pointed to one side and the third one pointed to the opposite side. We also located two low-lying neutral isomers (Figure S13). A C_s ($^2A'$) isomer is about 0.10 eV above the ground state. Another neutral isomer, C_1 (^2A), possesses an O double-bridge and is located 0.14 eV above the ground state.

4.3. $Ta_3O_n^-$ and Ta_3O_n ($n = 7-8$). The $Ta_3O_7^-$ anion ground state is C_1 (^1A) (Figure 8i), which is based on $Ta_3O_6^-$ by inserting an extra O to form a double-bridge. A higher symmetry C_{2v} ($^1A_1$) structure is about 0.11 eV above the ground state (Figure S14). The neutral ground state is C_s ($^2A'$) (Figure 9g), which is similar to the anion ground state. The $Ta_3O_8^-$ (C_{2v}, $^1A_1$) (Figure 8j) and Ta_3O_8 (C_s, $^2A'$) (Figure 9h) ground states are derived from those of $Ta_3O_7^{-/0}$ by attaching an extra O to form a double-terminal. An anion isomer C_{2v} ($^1A_1$) with two double-bridges is 0.16 eV above the anion ground state (Figure S16). Structures with a capping O atom are found substantially higher in energy for all $Ta_3O_n^-$ and Ta_3O_n ($n = 7-8$) species (Figures S14−S17).

5. Comparison between Experiment and Theory

The well-resolved PES data (Figures 1−7) serve as electronic fingerprint of the $Ta_3O_n^-$ ($n = 1-8$) clusters, allowing comparison with theoretical calculations and structural assignments.[45] The calculated ground-state VDEs are compared with the experimental values in Table 1, whereas the simulated PES spectra are compared with the 193 nm experimental data in Figure 10. As seen in Table 1, B3LYP underestimates the ground-state VDEs for $Ta_3O_n^-$. Typical discrepancies range from ~0.1 eV (for $Ta_3O_6^-$ and $Ta_3O_8^-$) to ~0.2 eV (for Ta_3O^-, $Ta_3O_2^-$, and $Ta_3O_4^-$); the largest discrepancy is ~0.3 eV for $Ta_3O_5^-$ and $Ta_3O_7^-$. For better comparison with the experimental spectra, in Figure 10 the simulated PES spectra are presented by aligning the first peak with the experimental band X or X′ (in cases of isomers for $n = 5$ and 6). The overall simulated PES patterns are in good agreement with the experimental spectra for all $Ta_3O_n^-$ clusters except for $Ta_3O_5^-$ and $Ta_3O_6^-$. For $Ta_3O_6^-$, it appears that both the singlet C_s ($^1A'$) and triplet C_{3v} ($^3A_1$) isomers are populated in roughly equal amount, resulting in the experimental bands X and A, and X′ and A′, respectively. The combination of the simulated spectra for the two isomers reproduces the experimental PES pattern reasonably well (Figures 10f and S23). For $Ta_3O_5^-$, the calculations favor a triplet state C_2 (^3A), but the simulated PES pattern for the lowest singlet state C_2 (^1A) appears to be in better agreement with the experiment (Figures 10e and S22), reproducing the three prominent bands X, A, and C. The triplet state C_2 (^3A) is probably responsible for the weak band B as a minor isomer, which should also contribute to other bands, in particular the broad band A. Additional simulations for low-lying $Ta_3O_n^-$ isomers (within ~0.3 eV) are shown in the Supporting Information (Figures S18−S25) as further confirmation for the assignments of the lowest energy structures.

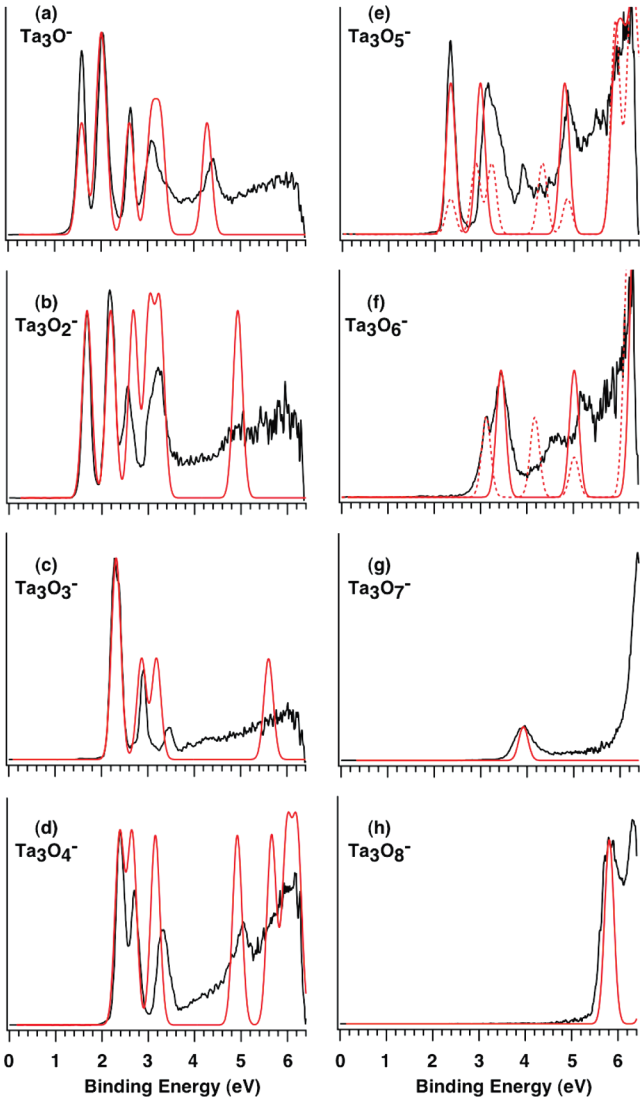

Figure 10. Simulated photoelectron spectra from the lowest-energy singlet structures (solid lines in red) for the $Ta_3O_n^-$ ($n = 1-8$) clusters and triplet structures (dashed lines in red) for $Ta_3O_5^-$ and $Ta_3O_6^-$ only, compared with the experimental spectra at 193 nm (solid lines in black). The simulations are done by fitting the distribution of calculated VDEs with unit-area Gaussian functions of 0.1 eV width. The simulated spectrum is shifted so that the first band maximum is aligned with the experimental spectrum.

The X band of $Ta_3O_3^-$ (Figure 3) is due to photodetachment from the fully occupied degenerate 1e′ MOs (Figure 11d). The 0.123 eV splitting resolved for this band (Figure 3a,b) is thus a final state effect because of the open-shell Ta_3O_3 neutral, and it could be due to either the Jahn−Teller effect or spin−orbit coupling. MO analysis shows that the 1e′ orbitals are primarily of Ta 6s character (Figure 11d) and a substantial spin−orbit splitting is unlikely. Therefore, the 0.123 eV splitting is most likely due to the Jahn−Teller effect in the Ta_3O_3 neutral. Indeed, the neutral Ta_3O_3 (C_s, $^2A'$) ground state has lower symmetry, in which the O atoms undergo out-of-plane distortions (Figure 9c). We also found a C_s ($^2A''$) state (Figure S7) ~0.11 eV above the ground state, which could correspond to the second component of the Jahn−Teller splitting.

6. Discussion

6.1. Structural Evolution of $Ta_3O_n^-$ ($n = 1-8$) Clusters. The good agreement between the experiment and theory lends support for ground-state structures for $Ta_3O_n^-$ ($n = 1-8$). For $Ta_3O_5^-$ and $Ta_3O_6^-$, two competitive isomers are observed. Starting from the triangular D_{3h} Ta_3^-, the first three O atoms ($n = 1-3$) successively occupy the bridging sites, one on each edge, reaching again a D_{3h} structure for $Ta_3O_3^-$. The next three O atoms ($n = 4-6$) successively occupy the terminal sites, one on each Ta. In $Ta_3O_7^-$ and $Ta_3O_8^-$, the additional O atoms form a double-bridge in $n = 7$ and a double-terminal in $n = 8$. Note that, among the $Ta_3O_n^-$ and Ta_3O_n ($n = 1-8$) ground state structures, only Ta_3O^-, Ta_3O, and $Ta_3O_3^-$ are planar; all other clusters are nonplanar with low symmetries. The planarity of Ta_3O^- and $Ta_3O_3^-$ is consistent with their relatively sharp PES features in comparison with those of the other clusters in the series. A previous infrared multiple photon dissociation spectroscopy study suggested that the structure of $Ta_3O_8^+$ cation involves a peroxo unit and a capped O site,[7] quite different from the $Ta_3O_8^-$ anion. This is because $Ta_3O_8^+$ is an electron deficient cluster, whereas $Ta_3O_8^-$ is stoichiometric.

6.2. Molecular Orbital Analyses and Sequential Oxidation. The MOs for the $Ta_3O_n^-$ ($n = 1-8$) anions are depicted in Figure 11 along with those for the bare Ta_3^- cluster for comparison. The ground state of Ta_3^- is a quintet state with four unpaired electrons (D_{3h}, $^5A_1'$) in the 1e″ and 2e′ MOs (Figure 11a).[29] In Ta_3^-, the $(1a_1')^2/(2e')^2$ and $(2a_1')^2/(1e')^4$ MOs form two σ bonding/antibonding pairs. The $(2a_1')^2/(1e')^4$ pair are fully occupied and do not contribute to net chemical bonding. The $(1a_2'')^2/(1e'')^2$ MOs form a π bonding/antibonding pair. The completely delocalized $(3a_1')^2$ MO is a δ bonding MO, rendering δ-aromaticity in Ta_3^- similar to that in $Ta_3O_3^-$.[14] The half-filled 2e′ and 1e″ MOs result in partial σ and π bonding in Ta_3^-, respectively. The MOs for the $Ta_3O_n^-$ clusters show close resemblance to those for Ta_3^-, with three-center Ta−Ta bonding for n up to 6 (Figure 11). Despite nonplanar and asymmetric coordination by the O atoms except in $Ta_3O_3^-$, the completely metal−metal bonding σ and π MOs provide stability for the Ta_3 framework. Although the ground state of Ta_3^- is open shell, the oxide anions are all closed shell except for $n = 5$ and 6, where a triplet state is competitive. The enhanced stability for the triplet C_{3v} ($^3A_1$) in $Ta_3O_6^-$ can be understood from MO analysis (Figure 11i): four Ta 6s/5d electrons occupy the completely bonding σ ($1a_1$) and degenerate bonding/antibonding σ (1e) MOs. The half-filling of the 1e MOs results in a triplet state and makes the triplet $Ta_3O_6^-$ σ-aromatic, according to the modified $4n$ aromatic-Hückel rule for triplet species.[46] Synthetic trinuclear tantalum compounds are rare, but examples are available ranging from 2-, to 6-, to 8-electron Ta_3 clusters.[30] In the $Ta_3O_n^-$ ($n = 0-8$) clusters, the oxidation state of the metal core is systematically tuned, from 16 electrons in Ta_3^- to zero in $Ta_3O_8^-$. The stability and bonding in the trinuclear Ta oxide clusters may be useful for understanding the synthetic compounds with similar trinuclear Ta cores.

The MOs shown in Figure 11 display a clear pattern of sequential oxidation in $Ta_3O_n^-$ as n increases from 0 to 7. The specific MOs from which the 2 electrons are transferred to O upon oxidation are marked with a square for $n = 0-5$. There are 16 valence 6s/5d electrons in Ta_3^-. Thus, $Ta_3O_8^-$ is a stoichiometric cluster, in which all the valence electrons are transferred to the O atoms, as shown in the valence MOs in Figure 12.

The $Ta_3O_7^-$ cluster is particularly interesting. It possesses two Ta 6s/5d electrons that occupy a completely localized 1a MO (Figure 11j). Our MO analysis shows that the 1a orbital contains 51% 5d + 25% 6s ($5d_{yz}$ mixed with 6s), which is localized on the Ta site coordinated by three O atom and gives rise to a Ta^{3+} site. Our PES spectrum (Figure 7a) shows that the localized

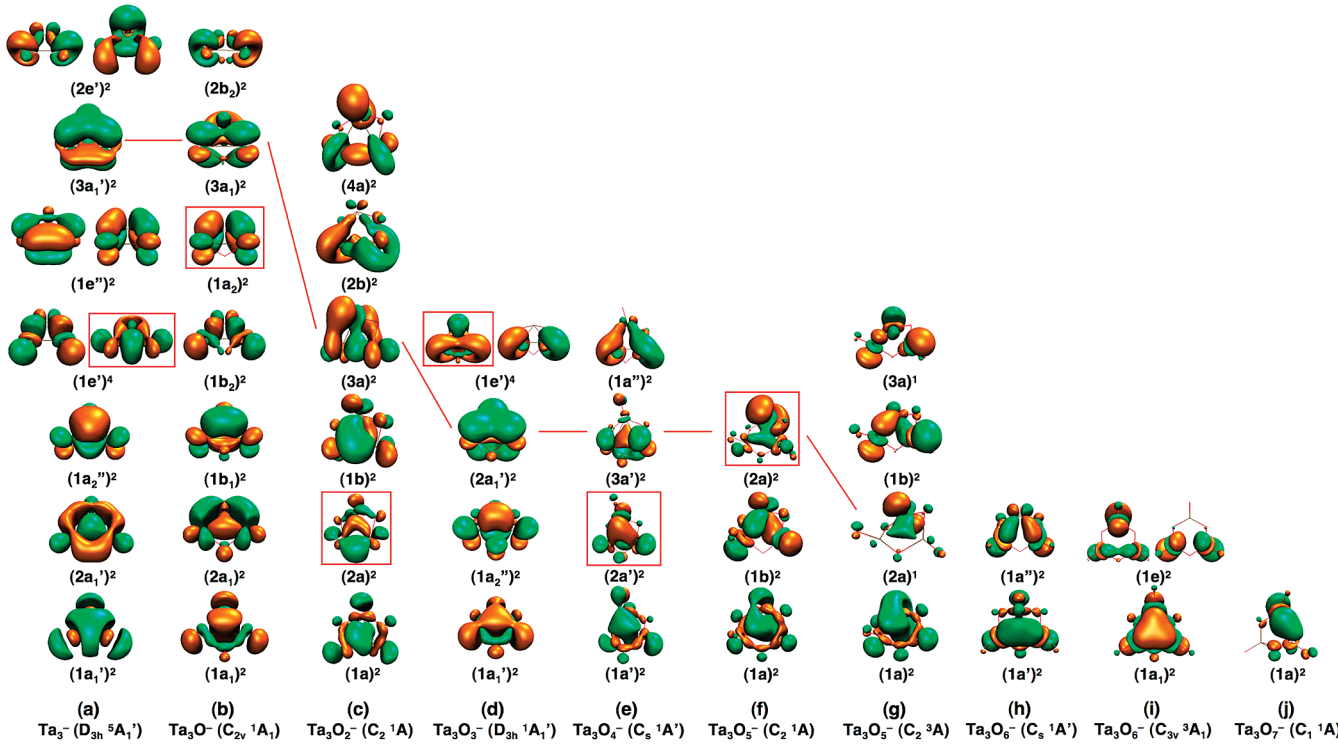

Figure 11. Pictures of the Ta-derived valence molecular orbitals for $Ta_3O_n^-$ ($n = 1-7$). The squares denote the orbitals from which two Ta 6s/5d electrons are transferred to O 2p upon sequential oxidation. The red lines trace the δ orbital in the series.

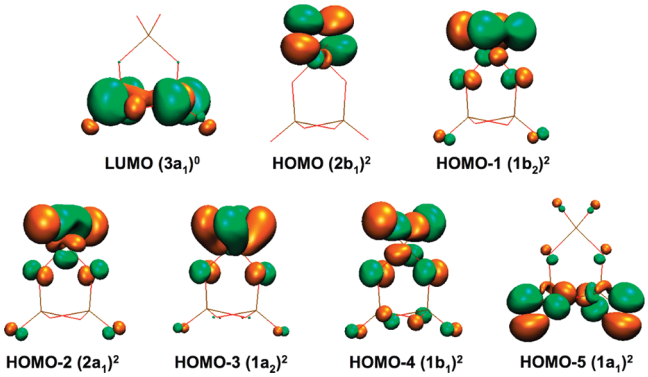

Figure 12. Frontier molecular orbital pictures for $Ta_3O_8^-$.

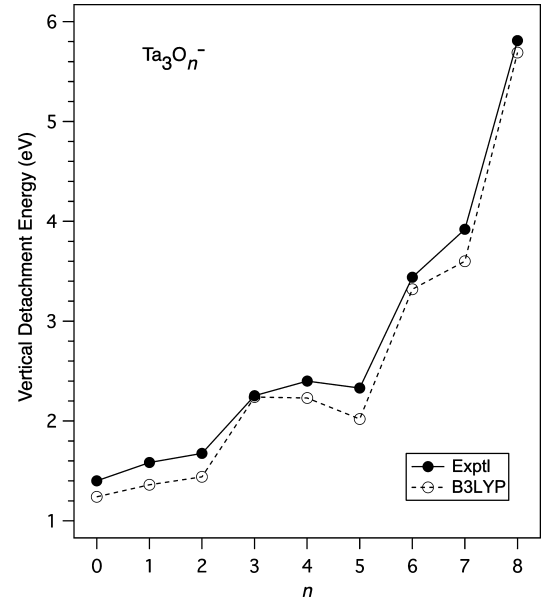

Figure 13. Experimental (solid line) and theoretical (dashed line) ground-state vertical detachment energies for $Ta_3O_n^-$ ($n = 0-8$) as a function of O content. Only the singlet states, C_2 (^{1}A) and C_s (^{1}A′), are shown for $Ta_3O_5^-$ and $Ta_3O_6^-$, respectively. The vertical detachment energy for Ta_3^- is taken from ref 29.

1a orbital (band X) is separated from the O 2p-type orbitals (band A) by ~2.4 eV. Thus, the localized Ta 6s/5d electron pair is expected to be chemically active and may serve as a molecular model for Ta^{3+} defect sites on oxide surfaces.

6.3. Trend of Electron Binding Energies as a Function of O Content. Figure 13 compares the experimental and calculated VDEs for the $Ta_3O_n^-$ ($n = 0-8$) series. The overall excellent agreement also lends considerable credence to the structures obtained for these oxide clusters. Surprisingly, the VDE trend as a function of O content in $Ta_3O_n^-$ is very different from other metal oxide clusters, such as in $Fe_mO_n^-$, $Cu_2O_n^-$, and $Al_3O_n^-$,[47] which display nearly linear increases as a function of n. The VDE trend in $Ta_3O_n^-$ seems to exhibit steps and jumps (Figure 13). The Ta_3^-, Ta_3O^-, and $Ta_3O_2^-$ species show similar VDEs within 0.3 eV; the $Ta_3O_3^-$, $Ta_3O_4^-$, and $Ta_3O_5^-$ species have similar VDEs within 0.2 eV; and the VDEs of $Ta_3O_6^-$ and $Ta_3O_7^-$ are within 0.5 eV. There is a large jump of 0.6 eV from $Ta_3O_2^-$ to $Ta_3O_3^-$, 1.1 eV from $Ta_3O_5^-$ to $Ta_3O_6^-$, and 1.9 eV from $Ta_3O_7^-$ to $Ta_3O_8^-$. The VDE trend can be qualitatively understood from the MO analysis in Figure 11 and is related to the nature of the HOMO. The HOMOs from $n =$ 0 to $n = 5$ are either antibonding or nonbonding, corresponding to their relatively low VDEs. On the other hand, the HOMOs of $n = 6$ and 7 involve a strongly Ta−Ta bonding orbital ($n =$ 6) and a localized orbital in $n = 7$, consistent with their significantly increased VDEs. The extremely high VDE of $Ta_3O_8^-$ is due to the detachment from O 2p type MOs (Figure 12).

6.4. On the δ Bonding in the $Ta_3O_n^-$ Clusters. Delocalized multicenter δ bonding (δ-aromaticity) represents a new mode of chemical bonding.[14,19,28,29] We have reported the δ-bonding

and δ-aromaticity in $Ta_3O_3^-$ previously.[14] Other $Ta_3O_n^-$ clusters also possess δ orbitals due to the d_{z^2} atomic orbital and allow us to follow the δ bonding with O content. The red lines in Figure 11 trace the δ orbitals in $Ta_3O_n^-$ clusters from $n = 0$ to $n = 5$. The δ orbital can be easily recognized in the cases of the D_{3h} Ta_3^- and $Ta_3O_3^-$. In other clusters, it is distorted or becomes localized. Although δ bonding is in general much weaker than σ or π bonding,[21] the delocalization of the δ orbital does provide additional stabilization. For example, the measured VDE from the δ orbital is 2.89 eV for $Ta_3O_3^-$, which is higher in comparison to 1.99, 2.57, 2.70, and 2.33 eV for Ta_3O^-, $Ta_3O_2^-$, $Ta_3O_4^-$, and $Ta_3O_5^-$, respectively, and can be attributed to the resonance effect. The trend of the binding energies for the δ orbital is also borne out from the theoretical calculations (Figure S27).

6.5. Terminal versus Bridging Oxygen Coordination in $Ta_3O_2^-$ and $Nb_3O_2^-$. We recently reported a C_1 (^{1}A) ground state for $Nb_3O_2^-$ with a unusual terminal O atom,[17] in which every Nb atom is unique with different oxidation states: 0, +1, and +3. A similar C_1 (^{1}A) structure is also located as a local minimum for $Ta_3O_2^-$ (Figure S26a), which is 0.56 eV above the C_2 (^{1}A) ground state (Figure 8b). We also found that the simulated PES spectrum for the C_1 (^{1}A) $Ta_3O_2^-$ (Figure S26b) deviates significantly from the experiment and it can be ruled out as the ground state for $Ta_3O_2^-$. The different ground state structures for $Ta_3O_2^-$ and $Nb_3O_2^-$ can be traced to the differences in the electronic structure of the monoxide species M_3O^- (M = Ta, Nb). The HOMO of M_3O^- is primarily an antibonding orbital of M 5s/6s character in both systems (Figure 11b for M = Ta). The second O atom is expected to interact strongly with either the HOMO ($2b_2$) or HOMO − 2 ($1a_2$) of M_3O^-, resulting in a terminal or bridging O ligand in $M_3O_2^-$, respectively. For M = Nb, the HOMO ($2b_2$) and HOMO − 2 ($1a_2$) show a sizable orbital energy difference (~1.4 eV),[17] and thus the second O atom primarily interacts with the HOMO, forming the unusual terminal Nb=O unit. In contrast, a significantly smaller HOMO and HOMO − 2 energy gap (~0.5 eV; Table S1) is observed for M = Ta. Consequently, its HOMO − 2 ($1a_2$) becomes energetically competitive to interact with the second O atom, resulting in a dibridged ground state for $Ta_3O_2^-$ (Figure 8b). The difference in the energy gap between HOMO ($2b_2$) and HOMO − 2 ($1a_2$) for Nb_3O^- versus Ta_3O^- may be attributed to the strong relativistic effects[48] in the Ta anion, whose 6s-based $2b_2$ orbital is energetically stabilized (by ~0.2 eV relative to Nb_3O^-) and 5d-based $1a_2$ orbital is destabilized (by ~0.7 eV relative to Nb_3O^-). The difference in the detailed electronic and geometric structures in the Nb and Ta oxide clusters is interesting and may also exist in other clusters of Ta and Nb.

7. Conclusions

Photoelectron spectroscopy is combined with density functional theory calculations to investigate the electronic and structural evolution, sequential oxidation, and chemical bonding in a series of tritantalum oxide clusters: $Ta_3O_n^-$ ($n = 1-8$). Well-resolved PES spectra are obtained for the anion clusters at various photon energies, allowing the access of all Ta 6s/5d metal-based electronic states. A unique trend of sequential oxidation is observed as a function of O content, but the electron binding energies are not linearly dependent on the number of O atoms. Extensive DFT calculations are performed at the B3LYP level in search of the lowest energy structures for both the anions and neutrals. Good overall agreement is achieved between the experimental and simulated PES spectra. The first three O atoms are found to successively occupy the bridging sites in the Ta_3 triangle. The next three O atoms successively occupy the three terminal sites. The seventh and eighth O atoms are shown to form a double-bridge and a double-terminal, respectively. Ta_3O^- and $Ta_3O_3^-$ are planar, but all other $Ta_3O_n^-$ clusters in the series are nonplanar. The multicenter δ bonding is observed in Ta_3O^- and $Ta_3O_3^-$. All the $Ta_3O_n^-$ ($n = 1-8$) clusters possess a closed shell singlet ground state, whereas for $n = 5$ and 6 both the singlet and triplet states are observed experimentally and they compete for the ground state. The $Ta_3O_7^-$ anion is shown to possess a localized Ta 6s/5d lone-pair, resulting in a Ta^{3+} center site, which may be a good model for reduced defect sites in bulk tantalum oxides.

Acknowledgment. The experimental work was supported by the Chemical Sciences, Geosciences and Biosciences Division, Office of Basic Energy Sciences, U.S. Department of Energy (DOE) under Grant DE-FG02-03ER15481 (catalysis center program), and performed at the W. R. Wiley Environmental Molecular Sciences Laboratory, a national scientific user facility sponsored by DOE's Office of Biological and Environmental Research and located at the Pacific Northwest National Laboratory, operated for DOE by Battelle. X.H. gratefully acknowledges support from the Natural Science Foundation of China (20641004 and 20771026) and the Natural Science Foundation of Fujian Province of China (No. 2008J0151).

Supporting Information Available: Comparison of the 193 nm photoelectron spectra for $Ta_3O_n^-$ ($n = 1-8$) (Figure S1), comparisons of experimental and calculated electron detachment energies (Tables S1−S4), alternative optimized anion and neutral cluster structures (Figures S2−S17) and their Cartesian coordinates (Table S5), simulated PES spectra from low-lying anion structures (Figures S18−S25), optimized $Ta_3O_2^-$ (C_1, ^{1}A) isomeric structure and its simulated photoelectron spectrum as compared with the 193 nm experimental spectrum (Figure S26), comparison of experimental and computational vertical detachment energies of the δ orbital in $Ta_3O_n^-$ ($n = 1-5$) as a function of O content (Figure S27), and complete ref 42. This material is available free of charge via the Internet at http://pubs.acs.org.

References and Notes

(1) (a) Wachs, I. E.; Chen, Y.; Jehng, J. M.; Briand, L. E.; Tanaka, T. *Catal. Today* **2003**, *78*, 13. (b) Wachs, I. E.; Briand, L. E.; Jehng, J. M.; Burcham, L.; Gao, X. *Catal. Today* **2000**, *57*, 323.

(2) Ushikubo, T. *Catal. Today* **2000**, *57*, 331.

(3) (a) Ushikubo, T.; Wada, K. *Appl. Catal.* **1990**, *67*, 25. (b) Ushikubo, T.; Wada, K. *J. Catal.* **1994**, *148*, 138. (c) Ushikubo, T.; Wada, K. *Appl. Catal., A* **1995**, *124*, 19. (d) Guiu, G.; Grange, P. *J. Catal.* **1995**, *156*, 132. (e) Tanaka, T.; Nojima, H.; Yamamoto, T.; Takenaka, S.; Funabiki, T.; Yoshida, S. *Phys. Chem. Chem. Phys.* **1999**, *1*, 5235. (f) Baltes, M.; Kytokivi, A.; Weckhuysen, B. M.; Schoonheydt, R. A.; Van Der Voort, P.; Vansant, E. F. *J. Phys. Chem. B* **2001**, *105*, 6211. (g) Samaranch, B.; de la Piscina, P. R.; Clet, G.; Houalla, M.; Gelin, P.; Homs, N. *Chem. Mater.* **2007**, *19*, 1445.

(4) Böhme, D. K.; Schwarz, H. *Angew. Chem., Int. Ed.* **2005**, *44*, 2336.

(5) (a) Zemski, K. A.; Bell, R. C.; Castleman, A. W., Jr. *Int. J. Mass Spectrom.* **1999**, *184*, 119. (b) Zemski, K. A.; Bell, R. C.; Castleman, A. W., Jr. *J. Phys. Chem. A* **2000**, *104*, 5732. (c) Zemski, K. A.; Justes, D. R.; Bell, R. C.; Castleman, A. W., Jr. *J. Phys. Chem. A* **2001**, *105*, 4410. (d) Zemski, K. A.; Justes, D. R.; Castleman, A. W., Jr. *J. Phys. Chem. A* **2001**, *105*, 10237.

(6) Green, S. M. E.; Alex, S.; Fleischer, N. L.; Millam, E. L.; Marcy, T. P.; Leopold, D. G. *J. Chem. Phys.* **2001**, *114*, 2653.

(7) Fielicke, A.; Meijer, G.; von Helden, G. *Eur. Phys. J. D* **2003**, *24*, 69.

(8) Molek, K. S.; Jaeger, T. D.; Duncan, M. A. *J. Chem. Phys.* **2005**, *123*, 144313.

(9) Dong, F.; Heinbuch, S.; He, S. G.; Xie, Y.; Rocca, J. J.; Bernstein, E. R. *J. Chem. Phys.* **2006**, *125*, 164318.

(10) Wu, Z. J.; Kawazoe, Y.; Meng, J. *THEOCHEM* **2006**, *764*, 123.

(11) Zheng, W. J.; Li, X.; Eustis, S.; Bowen, K. *Chem. Phys. Lett.* **2008**, *460*, 68.

(12) (a) Premaswarup, D.; Barrow, R. F. *Nature* **1957**, *180*, 602. (b) Weltner, W., Jr.; McLeod, D., Jr. *J. Chem. Phys.* **1965**, *42*, 882. (c) Cheetham, C. J.; Barrow, R. F. *Trans. Faraday Soc.* **1967**, *63*, 1835. (d) Brittain, R.; Powell, D.; Kreglewski, M.; Vala, M. *Chem. Phys.* **1980**, *54*, 71. (e) Dyke, J. M.; Ellis, A. M.; Feher, M.; Morris, A.; Paul, A. J.; Stevens, J. C. H. *J. Chem. Soc., Faraday Trans. 2* **1987**, *83*, 1555. (f) Ram, R. S.; Bernath, P. F. *J. Mol. Spectrosc.* **1998**, *191*, 125. (g) Zhou, M.; Andrews, L. *J. Phys. Chem. A* **1998**, *102*, 8251. (h) Chen, M.; Wang, X.; Zhang, L.; Yu, M.; Qin, Q. *Chem. Phys.* **1999**, *242*, 81. (i) Al-Khalili, A.; Hallsten, U.; Launila, O. *J. Mol. Spectrosc.* **1999**, *198*, 230. (j) Ram, R. S.; Bernath, P. F. *J. Mol. Spectrosc.* **2003**, *221*, 7. (k) Manke, K. J.; Vervoort, T. R.; Kuwata, K. T.; Varberg, T. D. *J. Chem. Phys.* **2008**, *128*, 104302.

(13) (a) Dolg, M.; Stoll, H.; Preuss, H.; Pitzer, R. M. *J. Phys. Chem.* **1993**, *97*, 5852. (b) Rakowitz, F.; Marian, C. M.; Seijo, L.; Wahlgren, U. *J. Chem. Phys.* **1999**, *110*, 3678. (c) Rakowitz, F.; Marian, C. M.; Seijo, L. *J. Chem. Phys.* **1999**, *111*, 10436.

(14) Zhai, H. J.; Averkiev, B. B.; Zubarev, D. Yu.; Wang, L. S.; Boldyrev, A. I. *Angew. Chem., Int. Ed.* **2007**, *46*, 4277.

(15) Zhai, H. J.; Döbler, J.; Sauer, J.; Wang, L. S. *J. Am. Chem. Soc.* **2007**, *129*, 13270.

(16) (a) Zhai, H. J.; Kiran, B.; Cui, L. F.; Li, X.; Dixon, D. A.; Wang, L. S. *J. Am. Chem. Soc.* **2004**, *126*, 16134. (b) Huang, X.; Zhai, H. J.; Waters, T.; Li, J.; Wang, L. S. *Angew. Chem., Int. Ed.* **2006**, *45*, 657. (c) Zhai, H. J.; Wang, L. S. *J. Am. Chem. Soc.* **2007**, *129*, 3022. (d) Zhai, H. J.; Li, S. G.; Dixon, D. A.; Wang, L. S. *J. Am. Chem. Soc.* **2008**, *130*, 5167.

(17) Zhai, H. J.; Wang, B.; Huang, X.; Wang, L. S. *J. Phys. Chem. A* **2009**, *113*, 3866.

(18) Huang, X.; Zhai, H. J.; Kiran, B.; Wang, L. S. *Angew. Chem., Int. Ed.* **2005**, *44*, 7251.

(19) Zubarev, D. Yu.; Averkiev, B. B.; Zhai, H. J.; Wang, L. S.; Boldyrev, A. I. *Phys. Chem. Chem. Phys.* **2008**, *10*, 257.

(20) Cotton, F. A.; Curtis, N. F.; Harris, C. B.; Johnson, B. F. G.; Lippard, S. J.; Mague, J. T.; Robinson, W. R.; Wood, J. S. *Science* **1964**, *145*, 1305.

(21) Cotton, F. A.; Murillo, C. A.; Walton, R. A. *Multiple Bonds Between Metal Atoms*, 3rd ed.; Springer: New York, 2005.

(22) Nguyen, T.; Sutton, A. D.; Brynda, M.; Fettinger, J. C.; Long, G. J.; Power, P. P. *Science* **2005**, *310*, 844.

(23) Gagliardi, L.; Roos, B. O. *Nature* **2005**, *433*, 848.

(24) Roos, B. O.; Borin, A. C.; Gagliardi, L. *Angew. Chem., Int. Ed.* **2007**, *46*, 1469.

(25) (a) Frenking, G. *Science* **2005**, *310*, 796. (b) Radius, U.; Breher, F. *Angew. Chem., Int. Ed.* **2006**, *45*, 3006. (c) Frenking, G.; Tonner, R. *Nature* **2007**, *446*, 276. (d) Weinhold, F.; Landis, C. R. *Science* **2007**, *316*, 61.

(26) (a) Brynda, M.; Gagliardi, L.; Widmark, P. O.; Power, P. P.; Roos, B. O. *Angew. Chem., Int. Ed.* **2006**, *45*, 3804. (b) La Macchia, G.; Brynda, M.; Gagliardi, L. *Angew. Chem., Int. Ed.* **2006**, *45*, 6210. (c) Roos, B. O.; Malmqvist, P.; Gagliardi, L. *J. Am. Chem. Soc.* **2006**, *128*, 17000. (d) Kreisel, K. A.; Yap, G. P. A.; Dmitrenko, O.; Landis, C. R.; Theopold, K. H. *J. Am. Chem. Soc.* **2007**, *129*, 14162. (e) Merino, G.; Donald, K. J.; D'Acchioli, J. S.; Hoffmann, R. *J. Am. Chem. Soc.* **2007**, *129*, 15295. (f) La Macchia, G.; Gagliardi, L.; Power, P. P.; Brynda, M. *J. Am. Chem. Soc.* **2008**, *130*, 5104. (g) Noor, A.; Wagner, F. R.; Kempe, R. *Angew. Chem., Int. Ed.* **2008**, *47*, 7246. (h) Nguyen, T.; Merrill, W. A.; Ni, C.; Lei, H.; Fettinger, J. C.; Ellis, B. D.; Long, G. J.; Brynda, M.; Power, P. P. *Angew. Chem., Int. Ed.* **2008**, *47*, 9115. (i) Tsai, Y.-C.; Hsu, C.-W.; Yu, J.-S. K.; Lee, G.-H.; Wang, Y.; Kuo, T.-S. *Angew. Chem., Int. Ed.* **2008**, *47*, 7250. (j) Hsu, C.-W.; Yu, J.-S. K.; Yen, C.-H.; Lee, G.-H.; Wang, Y.; Tsai, Y.-C. *Angew. Chem., Int. Ed.* **2008**, *47*, 9933. (k) Horvath, S.; Gorelsky, S. I.; Gambarotta, S.; Korobkov, I. *Angew. Chem., Int. Ed.* **2008**, *47*, 9937.

(27) (a) King, R. B. *Inorg. Chem.* **1991**, *30*, 4437. (b) Li, J. *J. Cluster Sci.* **2002**, *13*, 137. (c) Tsipis, A. C.; Tsipis, C. A. *J. Am. Chem. Soc.* **2003**, *125*, 1136. (d) Datta, A.; John, N. S.; Kulkarni, G. U.; Pati, S. K. *J. Phys. Chem. A* **2005**, *109*, 11647. (e) Wannere, C. S.; Corminboeuf, C.; Wang, Z. X.; Wodrich, M. D.; King, R. B.; Schleyer, P. v. R. *J. Am. Chem. Soc.* **2005**, *127*, 5701. (f) Chi, X. X.; Liu, Y. *Int. J. Quantum Chem.* **2007**, *107*, 1886.

(28) Averkiev, B. B.; Boldyrev, A. I. *J. Phys. Chem. A* **2007**, *111*, 12864.

(29) Wang, B.; Zhai, H. J.; Huang, X.; Wang, L. S. *J. Phys. Chem. A* **2008**, *112*, 10962.

(30) (a) King, R. B.; Braitsch, D. M.; Kapoor, P. N. *J. Am. Chem. Soc.* **1975**, *97*, 60. (b) Cotton, F. A.; Kibala, P. A.; Roth, W. J. *J. Am. Chem. Soc.* **1988**, *110*, 298. (c) Smith, M. D.; Miller, G. J. *J. Am. Chem. Soc.* **1996**, *118*, 12238. (d) Kawaguchi, H.; Tatsumi, K. *Organometallics* **1997**, *16*, 307. (e) Smith, M.; Miller, G. J. *J. Solid State Chem.* **1998**, *140*, 226.

(31) (a) Wang, L. S.; Cheng, H. S.; Fan, J. *J. Chem. Phys.* **1995**, *102*, 9480. (b) Wang, L. S.; Wu, H. In *Advances in Metal and Semiconductor Clusters, Vol. 4, Cluster Materials*; Duncan, M. A., Ed.; JAI Press: Greenwich, CT, 1998; pp 299−343.

(32) (a) Wang, L. S.; Li, X. In *Clusters and Nanostructure Interfaces*; Jena, P., Khanna, S. N., Rao, B. K., Eds.; World Scientific: Hackensack, NJ, 2000; pp 293−300. (b) Akola, J.; Manninen, M.; Hakkinen, H.; Landman, U.; Li, X.; Wang, L. S. *Phys. Rev. B* **1999**, *60*, R11297. (c) Wang, L. S.; Li, X.; Zhang, H. F. *Chem. Phys.* **2000**, *262*, 53. (d) Zhai, H. J.; Wang, L. S.; Alexandrova, A. N.; Boldyrev, A. I. *J. Chem. Phys.* **2002**, *117*, 7917.

(33) Becke, A. D. *J. Chem. Phys.* **1993**, *98*, 1372.

(34) Lee, C.; Yang, W.; Parr, R. G. *Phys. Rev. B* **1988**, *37*, 785.

(35) Stephens, P. J.; Devlin, F. J.; Chabalowski, C. F.; Frisch, M. J. *J. Phys. Chem.* **1994**, *98*, 11623.

(36) Andrae, D.; Haeussermann, U.; Dolg, M.; Stoll, H.; Preuss, H. *Theor. Chim. Acta* **1990**, *77*, 123.

(37) Küchle, W.; Dolg, M.; Stoll, H.; Preuss, H. Pseudopotentials of the Stuttgart/Dresden Group 1998, revision August 11, 1998; http://www.theochem.uni-stuttgart.de/pseudopotentiale.

(38) Martin, J. M. L.; Sundermann, A. *J. Chem. Phys.* **2001**, *114*, 3408.

(39) Dunning, T. H., Jr. *J. Chem. Phys.* **1989**, *90*, 1007.

(40) Kendall, R. A.; Dunning, T. H., Jr.; Harrison, R. J. *J. Chem. Phys.* **1992**, *96*, 6796.

(41) Tozer, D. J.; Handy, N. C. *J. Chem. Phys.* **1998**, *109*, 10180.

(42) Frisch, M. J.; et al. *Gaussian 03, revision D.01*; Gaussian, Inc.: Wallingford, CT, 2004.

(43) VMD (Visual Molecular Dynamics): Humphrey, W.; Dalke, A.; Schulten, K. *J. Mol. Graphics* **1996**, *14*, 33.

(44) (a) Zhai, H. J.; Wang, L. S.; Alexandrova, A. N.; Boldyrev, A. I.; Zakrzewski, V. G. *J. Phys. Chem. A* **2003**, *107*, 9319. (b) Zhai, H. J.; Bürgel, C.; Bonacic-Koutecky, V.; Wang, L. S. *J. Am. Chem. Soc.* **2008**, *130*, 9156.

(45) We have recently shown in a combined experimental and theoretical study that the B3LYP level of theory performs very well for the $Ta_3O_3^-$ cluster.[14] The current calculations on $Ta_3O_n^{-/0}$ ($n = 1-8$) were done using the same method and basis sets.

(46) Baird, N. C. *J. Am. Chem. Soc.* **1972**, *94*, 4941.

(47) (a) Wang, L. S.; Wu, H.; Desai, S. R. *Phys. Rev. Lett.* **1996**, *76*, 4853. (b) Wang, L. S.; Wu, H.; Desai, S. R.; Lou, L. *Phys. Rev. B* **1996**, *53*, 8028. (c) Wu, H.; Li, X.; Wang, X. B.; Ding, C. F.; Wang, L. S. *J. Chem. Phys.* **1998**, *109*, 449.

(48) Pyykkö, P. *Chem. Rev.* **1988**, *88*, 563.

JP905478W